Numerical solutions for nonlinear partial differential equations arising from modelling dye-sensitized solar cells

B. Maldon[1] B. P. Lamichhane[2] N. Thamwattana[3]

(Received 26 February 2019; revised 14 October 2019)

Abstract

Dye-sensitized solar cells have generated diverse research directions, which include a mathematical model based on the diffusion of electrons in the conduction band of a nano-porous semiconductor (traditionally TiO_2). We solve the nonlinear diffusion equation under its boundary conditions, as stated by Anta et al. [J. Phys. Chem. B 110 (2006) pp 5372–5378]. We employ a standard finite difference method, a fourth order finite difference method scheme and a Runge–Kutta scheme. We calculate errors and evaluate the utility of each scheme as it applies to this boundary value problem.

DOI:10.21914/anziamj.v60i0.14053 gives this article, © Austral. Mathematical Soc. 2019. Published October 23, 2019, as part of the Proceedings of the 18th Biennial Computational Techniques and Applications Conference. ISSN 1445-8810. (Print two pages per sheet of paper.)

Contents

1 Introduction

O'Regan and Grätzel's foundational 1991 paper [5] introduced dye sensitized solar cells (DSSCs) as a viable alternative for renewable energy. By replacing costly silicon semiconductors found in typical solar cells with nanoporous semiconductors and photosensitive dye, DSSCs are able to provide sunlight-induced power at a significantly lower cost.

A DSSC is comprised of four primary materials: the photosensitive dye, the nanoporous semiconductor, the counter electrode, and the electrolyte couple. During operation, the photosensitive dye donates its electrons to the nanoporous semiconductor in a sunlight-induced process known as electron injection [5]. Injected electrons power a load before being reintroduced into the DSSC by a counter electrode. Finally, the electrolyte couple returns electrons from the counter electrode to the photosensitive dye by a redox reaction. DSSCs are also subject to loss mechanisms (known as recombination), such as regeneration of the photosensitive dye or electrolyte couple by the nanoporous semiconductor. Recombination reactions harm the electron generation process by preventing electrons from leaving the DSSC to power a load as intended.

In 1994, Södergren et al. [6] proposed a linear ordinary differential equation (ODE) for modelling the conduction band electron density in the nanoporous semiconductor of a DSSC. This was the first mathematical model to specifically model DSSCs, as previous models had been inherited from other solar cells. Later, Cao et al. [2] proposed a partial differential equation (PDE) by adding time-dependence to create a diffusion-like model. A nonlinear variant of the PDE emerged in 2006 [1], built to capture the role of nonlinear diffusion in DSSCs [3].

Mathematical model

Given a DSSC of thickness d, the conduction band electron density $n(x,t)$ at depth $x \in [0,d]$ and time $t \geqslant 0$ satisfies [1]

$$\frac{\partial n}{\partial t} = D_0 \frac{\partial}{\partial x}\left[\left(\frac{n(x,t)}{n_{eq}}\right)^{\beta} \frac{\partial n}{\partial x}\right] + \varphi_0 e^{-\alpha x} - k_R \left(\frac{n(x,t)}{n_{eq}}\right)^{\beta} [n(x,t) - n_{eq}], \tag{1}$$

where D_0 is the diffusion coefficient, n_{eq} is the dark equilibrium electron density, φ_0 is the incident photon flux, α is the absorption coefficient of the ruthenium (II) dye, k_R is the recombination coefficient and β is the diffusion order. This PDE is subject to the boundary conditions

$$n(0,t) = n_{eq} \quad \text{and} \quad \left.\frac{\partial n}{\partial x}\right|_{x=d} = 0, \tag{2}$$

and the initial condition

$$n(x,0) = n_{eq}. \tag{3}$$

We non-dimensionalise the model with the same parameter scalings as Cao et al. [2]:

$$\bar{n} = \frac{n}{n_{eq}}, \quad \bar{x} = \frac{x}{d}, \quad \bar{t} = \frac{D_0 t}{d^2}. \tag{4}$$

Table 1: Parameter values for DSSC model.

Parameter	Value
μ	25
ν	5
ξ	10^{-5}

The non-dimensional equation is therefore

$$\frac{\partial \bar{n}}{\partial \bar{t}} = \frac{\partial}{\partial \bar{x}}\left(\bar{n}^{\beta}\frac{\partial \bar{n}}{\partial \bar{x}}\right) + \mu e^{-\nu \bar{x}} - \xi \bar{n}^{\beta}\left(\bar{n} - 1\right), \tag{5}$$

where our non-dimensional parameters are $\mu = d^2\varphi_0/D_0 n_{eq}$, $\nu = \alpha d$ and $\xi = k_R d^2/D_0$. Dropping the bar notation, the boundary and initial conditions become

$$n(x,0) = 1, \quad n(0,t) = 1, \quad \left.\frac{\partial n}{\partial x}\right|_{x=1} = 0.$$

The values for the non-dimensional parameters are given in Table 1 and are based on data provided by Anta et al. [1] and Gacemi et al. [4]. Unless otherwise stated, all numerical results computed in this article use the data in Table 1.

In this article, we numerically solve PDE (5) for $\beta = 1$. If $\beta = 0$, then the PDE collapses to a linear equation that is readily solved analytically. Figure 1 plots n_{exact}, the exact solution of (5) for $\beta = 0$, over times $t \in [0,1]$. To verify the effectiveness of our numerical simulations, we compare the numerical solution for the $\beta = 0$ special case with the exact solution. For the nonlinear case $\beta = 1$, we compute the error using the numerical solution under an extremely fine grid to represent a pseudo-exact solution.

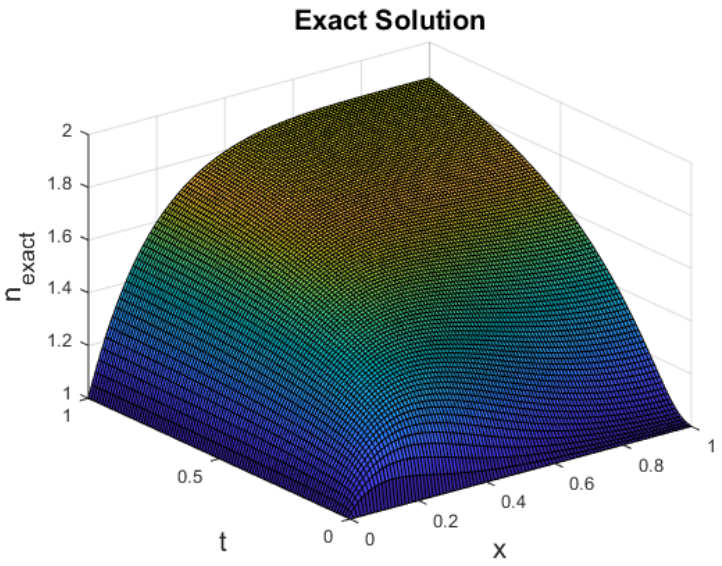

Figure 1: Solution n_{exact} of (5) against x and t for the $\beta = 0$ special case.

2 Finite difference method

For our first scheme, we devise a standard forward time central space finite difference method (FDM). We begin with a spatial discretisation of $[0, 1]$ into N_x nodes and a temporal discretisation $[0, T]$ into N_t nodes, where T is the final simulation time. In this article, $u_{i,j}$ represents the numerical solution of (1) at $x = (j-1)\Delta x$ and $t = (i-1)\Delta t$, where $\Delta x = 1/(N_x - 1)$ and $\Delta t = T/(N_t - 1)$.

The boundary conditions specify the nodes on the boundary of $[0, 1]$, so we approximate the spatial derivatives at node (i, j) for $i \in \{1, \cdots, N_t\}$ and $j \in \{1, \cdots, N_x\}$ by

$$\left(\frac{\partial n}{\partial x}\right)_{i,j} \approx \frac{u_{i,j+1} - u_{i,j-1}}{2\Delta x}, \quad \left(\frac{\partial^2 n}{\partial x^2}\right)_{i,j} \approx \frac{u_{i,j+1} - 2u_{i,j} + u_{i,j-1}}{\Delta x^2}.$$

To account for the boundary condition at $x = 1$, for every time step i we introduce a 'ghost node' at $x = 1 + \Delta x$ defined by

$$u_{i,N_x+1} = u_{i,N_x-1},$$

so that the central difference approximation of $\partial n/\partial x$ at $x = 1$ agrees with the boundary condition. We approximate the temporal derivative at node (i, j) by a standard forward difference

$$\left(\frac{\partial n}{\partial t}\right)_{i,j} \approx \frac{u_{i+1,j} - u_{i,j}}{\Delta t}.$$

Results Figure 2 plots the numerical solution of equation (1) for $\beta = 1$ and for $T = 0.004$ and $T = 1$. As the system evolves from the constant equilibrium of the initial condition, we see the exponential source term sharply increases the electron density near $x = 0$. The resulting peak is an interaction between the diffusion coefficient, the exponential source term and the boundary condition at $x = 0$.

The finite difference method presents consistently small errors, despite having the lowest order of the numerical schemes considered in this article. We attribute this to the extreme magnitude of the higher order spatial and temporal derivatives of the exact solution, which suggest that higher order schemes may encounter regularity issues.

3 Fourth order spatial discretisation

For our second scheme, we increase stability by estimating the spatial derivatives with five points, in contrast to the two used in the central difference

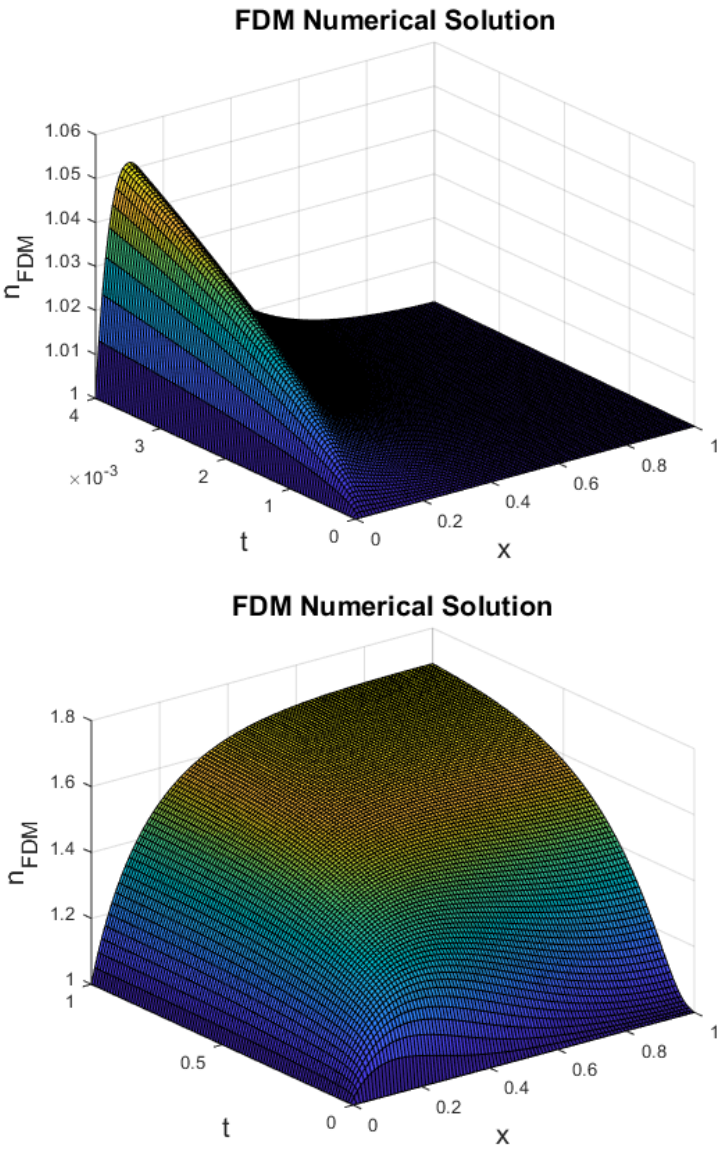

Figure 2: Numerical solution $n(x,t)$ of (1) against x and t, for $\beta = 1$ under the FDM scheme, for (top) $T = 0.004$ and (bottom) $T = 1$.

scheme. Letting $c = 1/\Delta x$, for $j \in \{3, ..., N_x - 2\}$ we set up estimates

$$\left(\frac{\partial n}{\partial x}\right)_{i,j} \approx \frac{c}{12}u_{i,j-2} - \frac{2c}{3}u_{i,j-1} + \frac{2c}{3}u_{i,j+1} - \frac{c}{12}u_{i,j+2}\,,$$
$$\left(\frac{\partial^2 n}{\partial x^2}\right)_{i,j} \approx -\frac{c^2}{12}u_{i,j-2} + \frac{4c^2}{3}u_{i,j-1} - \frac{5c^2}{2}u_{i,j} + \frac{4c^2}{3}u_{i,j+1} - \frac{c^2}{12}u_{i,j+2}\,.$$

where the coefficients have been determined so that the first spatial derivative of quartic polynomials is estimated exactly. Since this scheme is incompatible with $j = 2$ and $N_x - 1$, we set up modified schemes for these nodes:

$$\left(\frac{\partial n}{\partial x}\right)_{i,2} \approx -\frac{c}{4}u_{i,1} - \frac{5c}{6}u_{i,2} + \frac{3c}{2}u_{i,3} + \frac{c}{3}u_{i,4} - \frac{c}{12}u_{i,5}\,,$$
$$\left(\frac{\partial^2 n}{\partial x^2}\right)_{i,2} \approx \frac{11c^2}{12}u_{i,1} - \frac{5c^2}{3}u_{i,2} + \frac{c^2}{2}u_{i,3} + \frac{c^2}{3}u_{i,4} - \frac{c^2}{12}u_{i,5}\,,$$
$$\left(\frac{\partial n}{\partial x}\right)_{i,N_x-1} \approx \frac{c}{4}u_{i,N_x-4} - \frac{4c}{3}u_{i,N_x-3} + 3cu_{i,N_x-2} - 4cu_{i,N_x-1} + \frac{25c}{12}u_{i,N_x}\,,$$
$$\left(\frac{\partial^2 n}{\partial x^2}\right)_{i,N_x-1} \approx \frac{11c^2}{12}u_{i,N_x-4} - \frac{14c^2}{3}u_{i,N_x-3} + \frac{19c^2}{2}u_{i,N_x-2} - \frac{26c^2}{3}u_{i,N_x}\,.$$

Finally, we use a five-point scheme to estimate $\partial n(1,t)/\partial x$, once again choosing coefficients so that this spatial derivative at $x = 1$ is estimated exactly for quartic polynomials. Given the boundary condition $\partial n(1,t)/\partial x = 0$, we rearrange to obtain

$$u_{i,N_x} = -\frac{3}{25}u_{i,N_x-4} + \frac{16}{25}u_{i,N_x-3} - \frac{36}{25}u_{i,N_x-2} + \frac{48}{25}u_{i,N_x-1}\,.$$

Results Figure 3 plots the numerical solution of equation (1) for $\beta = 1$ and for $T = 0.004$ and $T = 1$.

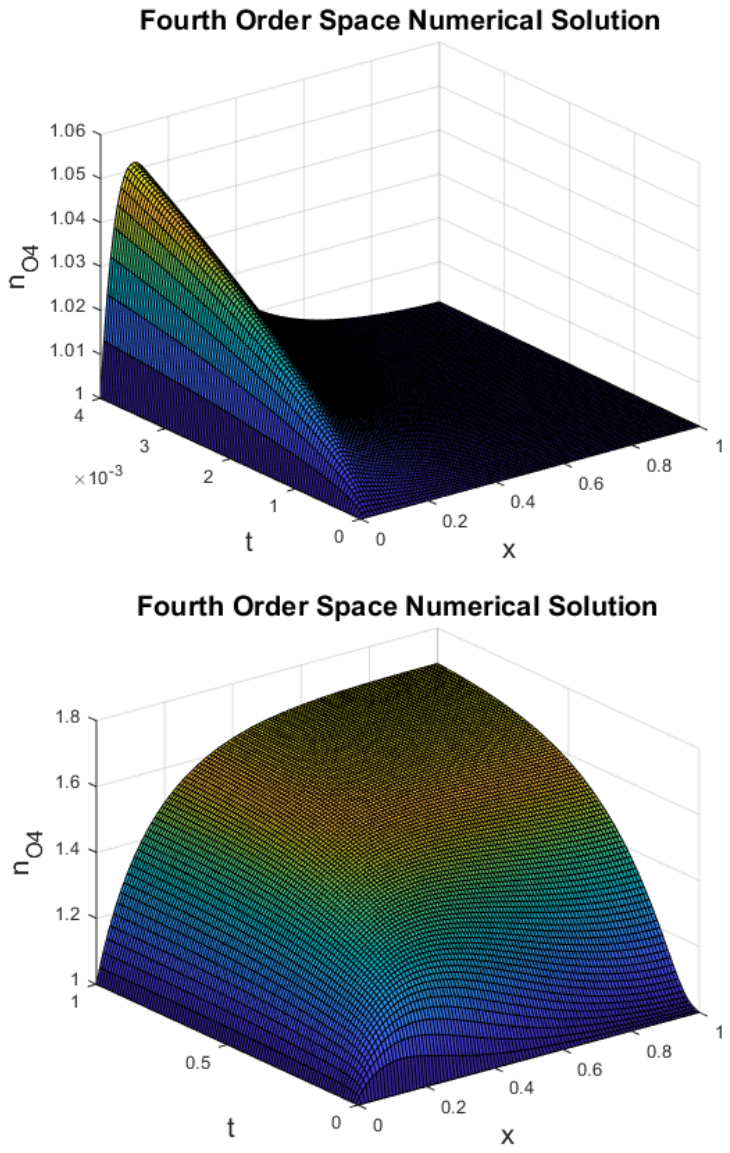

Figure 3: Numerical solution $n(x,t)$ of (1) against x and t for $\beta = 1$ under the fourth order space scheme and forward Euler time for (top) $T = 0.004$ and (bottom) $T = 1$.

4 Runge–Kutta Method

For our final scheme, we consider a fourth order Runge–Kutta (RK4) iteration under the same fourth order spatial discretisation used in Section 3. This results in a system of N_x ODEs dependent on t, which we solve with a method of lines approach and Runge–Kutta iteration in time. We choose a fourth order spatial discretisation so that our numerical scheme is fourth order in both space and time.

Results Figure 4 plots the numerical solution of equation (1) for $\beta = 1$ and for $T = 0.004$ and $T = 1$.

Concerning errors, given a sufficiently fine grid we obtain smaller errors than for the standard FDM scheme. Table 2 shows that grid refinement gives a substantial improvement initially, and then substantially less improvement with even finer grids.

5 Comparison of results

To compare each numerical scheme, we run simulations on progressively finer grids. From these computations we interpolate solutions on even finer grids and verify that the error is vanishing with increased grid resolution. That is, given a coarse grid with numerical solution u_c and an interpolated fine-grid solution u_f, the error ϵ is

$$\epsilon = \|u_f - u_c\| \sqrt{\Delta x \Delta t}\,, \tag{6}$$

where Δx and Δt are calculated in the coarse grid. The norms are calculated with MATLAB's usual norm function. For all error computations we simulate on $t \in [0, 0.004]$ to reduce calculation time. Table 2 gives the errors for different numbers of spatial nodes and $N_t = 100 N_x$ for each grid.

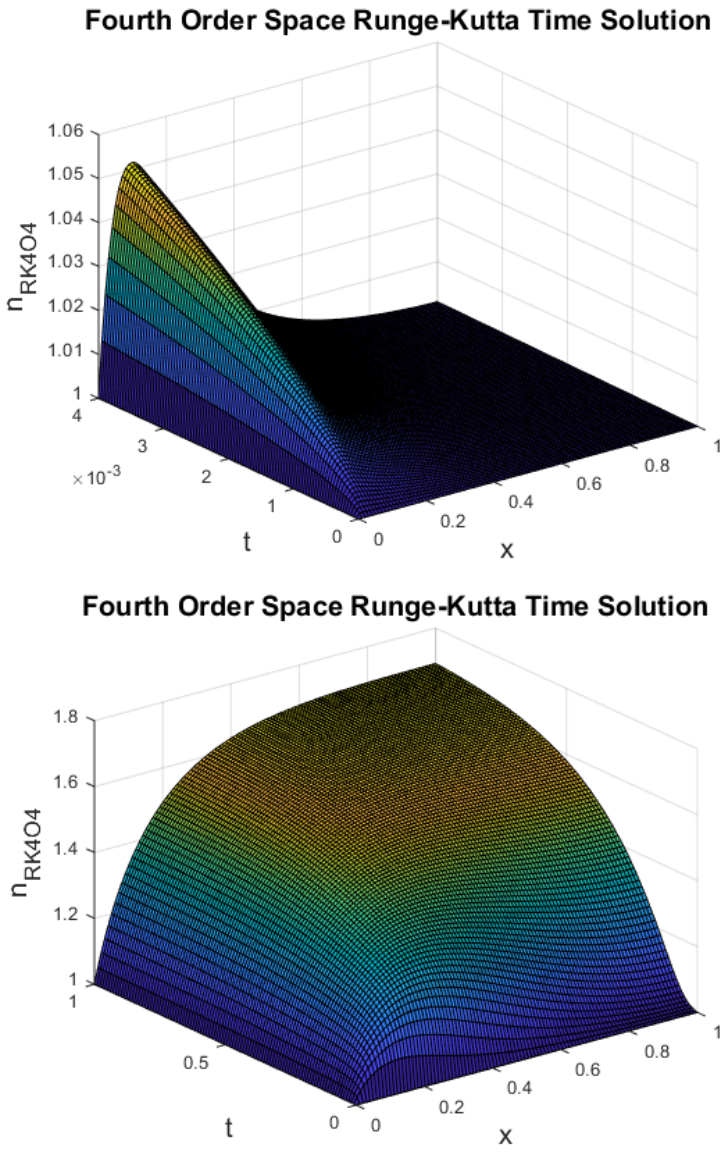

Figure 4: Numerical solution $n(x,t)$ of (1) against x and t, for $\beta = 1$ under the Runge–Kutta scheme for (top) $T = 0.004$ and (bottom) $T = 1$.

Table 2: Errors for the standard FDM and fourth order Runge–Kutta (RK4) scheme under grid refinement ($\beta = 1$).

	$N_x = 25$	$N_x = 50$	$N_x = 100$	$N_x = 200$	$N_x = 400$
FDM	1.43×10^{-5}	3.55×10^{-6}	8.53×10^{-7}	1.95×10^{-7}	3.67×10^{-8}
RK4	5.90×10^{-6}	5.70×10^{-7}	1.12×10^{-7}	2.78×10^{-8}	2.32×10^{-8}

Table 3: Parameter values for DSSC model provided by Cao et al. [2].

Parameter	Value
μ	1000
ν	10
ξ	0

Figure 5 shows that the Runge–Kutta scheme faces a regularity complication as the temporal derivatives of the exact solution for the $\beta = 0$ special case are of the order 10^{10} and 10^{12} in magnitude. We compute these derivatives for the special case $\beta = 0$ so we can use the exact solution rather than one of the numerical schemes. Consequently, we do not obtain the fourth order convergence shown in Table 2 for the fourth order schemes that the theory would otherwise predict. Furthermore, we find an explanation as to why the standard FDM scheme performs so well, as it is unaffected by these derivatives.

Figure 6 provides a direct comparison of a simulation by Cao et al. [2, Fig. 6(a)] with our equivalent numerical solution. For this simulation, we use the same data as Cao et al. [2] specified in Table 3. Both simulations are over $t \in [0, 1]$. In our simulation we used 100 spatial nodes and 200 000 temporal nodes.

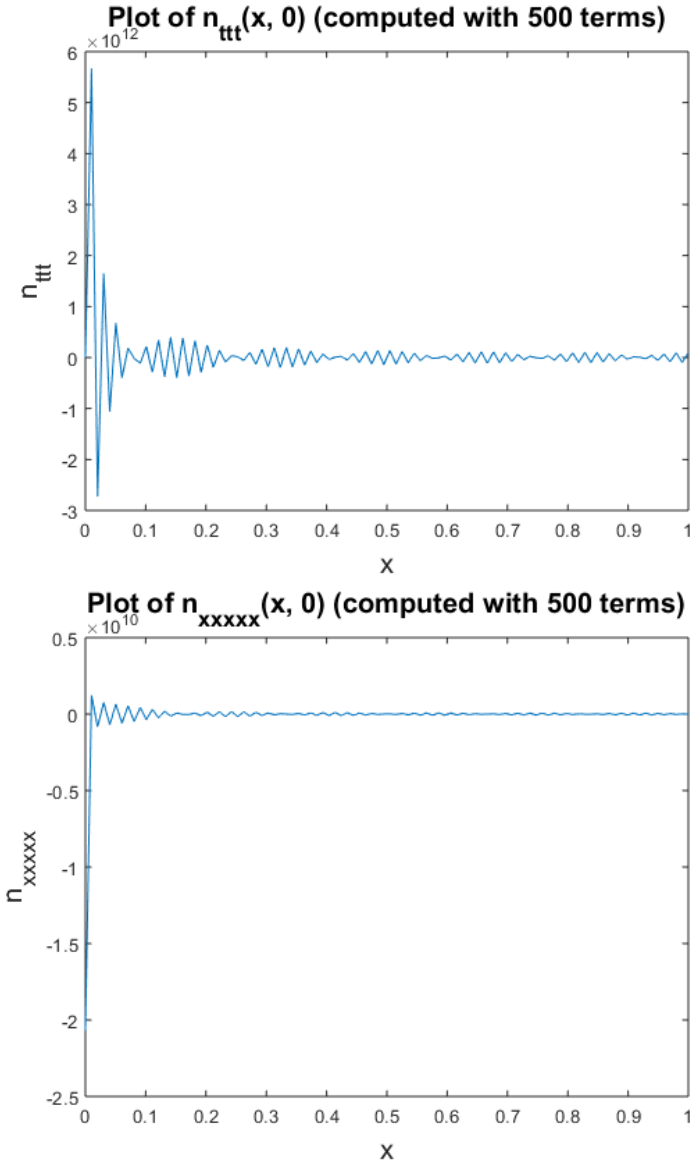

Figure 5: Plots of (top) $\partial^3 u(x,0)/\partial t^3$ and (bottom) $\partial^5 u(x,0)/\partial t^5$ for the exact solution ($\beta = 0$) of (5).

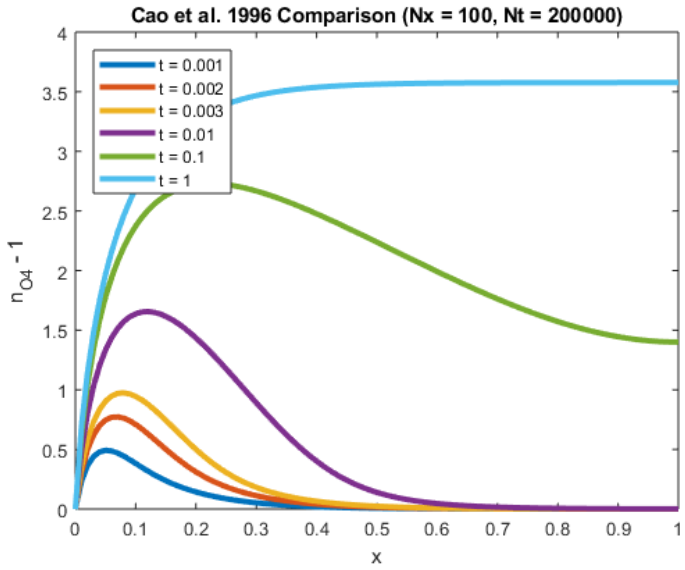

Figure 6: Numerical solution of (1) using data from Table 3 for comparison with a simulation by Cao et al. [2, Fig. 6(a)].

6 Conclusion

We have devised three numerical schemes for numerically solving a partial differential equation arising from the modelling of dye-sensitised solar cells. All numerical schemes present extremely small errors given a sufficient grid size (showing errors of the order of 10^{-8} with a $400 \times 40\,000$ grid). We obtain second order convergence for the standard FDM scheme, as expected, but no significant improvement in the convergence rate for the other schemes. The discrepancy is explained by the exact solution of the linear special case of (1). Finally, we find our schemes compare favourably with simulations by other authors.

Acknowledgements This research was conducted with the support of the Australian Government Research Training Program Scholarship. The authors are grateful to the Australian Research Council for funding via Discovery Project DP170102705.

References

[1] J. A. Anta, F. Casanueva, and G. Oskam. "A numerical model for charge transport and recombination in dye-sensitized solar cells". In: *J. Phys. Chem. B* 110.11 (2006), pp. 5372–5378. DOI: 10.1021/jp056493h (cit. on pp. C233, C234).

[2] F. Cao, G. Oskam, G. J. Meyer, and P. C. Searson. "Electron transport in porous nanocrystalline TiO_2 photoelectrochemical cells". In: *J. Phys. Chem.* 100.42 (1996), pp. 17021–17027. DOI: 10.1021/jp9616573 (cit. on pp. C233, C242, C244).

[3] A. J. Frank, N. Kopidakis, and J. van de Lagemaat. "Electrons in nanostructured TiO_2 solar cells: transport, recombination and photovoltaic properties". In: *Coordin. Chem. Rev.* 248 (2004), pp. 1165–1179. DOI: 10.1016/j.ccr.2004.03.015 (cit. on p. C233).

[4] Y. Gacemi, A. Cheknane, and H. S. Hilal. "Simulation and modelling of charge transport in dye-sensitized solar cells based on carbon nano-tube electrodes". In: *Phys. Scripta* 87.3 (2013), pp. 035703–035714. DOI: 10.1088/0031-8949/87/03/035703 (cit. on p. C234).

[5] B. O'Regan and M. Grätzel. "A low-cost, high-efficiency solar cell based on dye-sensitized colloidal TiO_2 films". In: *Nature* 353 (1991), pp. 737–740. DOI: 10.1038/353737a0 (cit. on p. C232).

[6] S. Södergren, A. Hagfeldt, J. Olsson, and S. Lindquist. "Theoretical models for the action spectrum and the current-voltage characteristics of microporous semiconductor films in photoelectrochemical cells". In: *J. Phys. Chem.* 98 (1994), pp. 5552–5556. DOI: 10.1021/j100072a023 (cit. on p. C233).

Author addresses

1. **B. Maldon**, School of Mathematical and Physical Sciences, University of Newcastle, New South Wales 2308, Australia.
mailto:benjamin.maldon@uon.edu.au
orcid:0000-0001-8746-7575
2. **B. P. Lamichhane**, School of Mathematical and Physical Sciences, University of Newcastle, New South Wales 2308, Australia.
3. **N. Thamwattana**, School of Mathematical and Physical Sciences, University of Newcastle, New South Wales 2308, Australia.